Venting dynamics of an immersed granular layer

Germán Varas, Valérie Vidal, and Jean-Christophe Géminard
Laboratoire de Physique, Université de Lyon, Ecole Normale Supérieure – CNRS, 46 Allée d'Italie, 69364 Lyon Cedex, France
(Received 21 July 2010; revised manuscript received 16 December 2010; published 28 January 2011)

Air is injected locally at the base of an immersed granular bed. The gas, which is forced to flow gently through the material, creates several paths between the grains. We observe that the latter gas venting results in the emission of bubbles in a localized region at the free surface. Additional experiments, performed in two dimensions, permit a direct visualization of the paths, and a theoretical approach shows that the typical size of the region at the free surface can be accounted for by a diffusionlike process. The diffusion coefficient is expressed as a function of the system parameters.

DOI: 10.1103/PhysRevE.83.011302 PACS number(s): 83.80.Fg, 47.57.Gc, 47.85.Dh

I. INTRODUCTION

Fluid venting at the seafloor, usually concentrated along ocean margins, is a widely recognized phenomenon of geophysical, biophysical, and economical importance. On the one hand, the gas emitted is mainly hydrocarbon, whose extraction is of obvious economic interest [1,2]. On the other hand, the ecosystem on the seafloor close to the vents benefits greatly from the minerals brought by the gas or fluid emission [3]. Understanding the flowing regimes through a sediment layer is also fundamental from a geophysics point of view. Indeed, flow regimes in saturated granular media can go from homogeneous seepage (fluid percolation) to piping and partial failure [4]. This last case plays a major role in soil liquefaction, mud volcanism and diapirism, and hydraulic fracture [1,5].

The onset of piping phenomena, and its subsequent dynamics, has been studied extensively in the case of a two-phase flow (fluid and grains), both in physics and geophysics [4,6–8]. It has been found that the channels are not stationary, but migrate across the surface, forming a complex subsurface plumbing system exhibiting different morphologies, representative of the fluid-venting dynamics [9]. At longer times, the channel migration fluidizes the region surrounding the loci of the gas emission, eventually leading to massive instabilities of water-saturated grounds [4].

Three-phase systems (solid, liquid, and gas) present an even more complex dynamics that has not been fully characterized up to now. For instance, in a two-dimensional (2D) porous medium that is not altered by the gas flow, one observes a transition in the morphology of the invasion front [10]. In granular systems, in which the grains are likely to move under the action of the gas flow (unconstrained immersed granular layer), three different regimes have been reported: a continuous bubbling regime during which one observes an almost periodic emission of gas bubbles at the free surface, an open-channel regime associated with a continuous gas emission through a stable channel that crosses the whole system, and an intermittent regime that corresponds to a spontaneous alternation of the degassing regime between the bubbling and the open-channel regimes [11–13]. Such dynamics is reminiscent of complex fluids, such as gels or polymers [14,15], crossed by ascending air flows.

In the present paper, we investigate the bubbling pattern that results from the gentle, punctual, injection of a gas at the base of an immersed granular layer. In this regime, the gas flow does not necessarily induce a significant motion of the grains. First, we characterize the gas-emission loci at the free surface of a cylindrical bed. Second, we report direct observations, in a 2D experiment, of the paths created by the gas in the bulk of the material. Finally, we show that a diffusionlike process accounts for the experimental observations and we relate the associated diffusion coefficient to the parameters of the problem.

II. SETUP AND PROTOCOL

The experiment consists in gently injecting air at the base of a column of immersed grains and observing the loci of the resulting bubble emissions at the free surface. The setup consists of a Plexiglas cylindrical tank (24 cm diameter) whose bottom is pierced at the center by an inlet hole (2 mm diameter) through which air is injected (Fig. 1). A reducing valve and a capillary tube are used to ensure that air is injected at a constant, small flow rate, Φ, in a chamber of volume V, connected to the inlet (provided that the pressure drop in the capillary tube is much larger than the fluctuations of the pressure inside the chamber, the flow rate is not significantly altered by the dynamics of the granular layer and remains constant). The flow rate Φ (ranging from 1 to 3 mL/s) is tuned by changing either the capillary tube (rough) or the pressure difference imposed by the reducing valve (fine) and is subsequently measured (to within 0.1 mL/s) by means of a homemade flow meter.

The initial condition is obtained as follows: the cylinder is filled with glass beads (USF Matrasur, sodosilicated glass) previously sieved in order to control their size (diameter $d =$ 150–250, 250–425, and 425–600 μm). The height of the granular bed h_g ranges from 2 to 24 cm. Distilled water is added and the material is vigorously stirred with a paddle to eliminate the gas bubbles trapped inside. The free surface of the granular bed is leveled and the water height above is $h_w \sim 1$ cm, which prevents the rising bubbles from hiding the emission locus.

Then, air injection is initiated by setting the flow rate Φ to a chosen value. Air passes through the system and we observe at the surface a series of bubble emissions. To determine the loci of the gas emission, which vary in time, the free surface is imaged by means of a webcam (Logitech, QuickCam S7500) connected to a PC. The light source consists of a transparency flat viewer (Just NormLicht, Classic Line) placed slightly

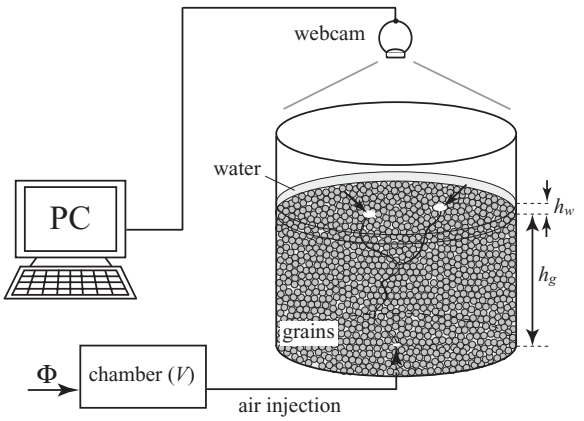

FIG. 1. Experimental setup: Air is injected at a constant flow rate Φ into a chamber of volume V connected to the bottom of an immersed granular column (h_g is the height of the granular column and h_w is the height of the water above). The loci of the gas emission are determined by imaging the free surface by means of a webcam.

out-of-axis to avoid direct reflections from the liquid surface into the camera. In such conditions, the emission of a bubble is marked by the appearance of a dark dot in the image of the free surface (Fig. 2, inset). A free software (Astra Image Webcam Video Grabber) is used to take 20 images per second with a resolution of 640 × 480 pixels. An automatic detection (Matlab, MathWorks) makes it possible to determine the loci of the gas emission with an accuracy of about 2 mm.

In the following sections, we report results obtained for 10-min acquisitions for different heights of grains h_g, flow rate Φ, and grain size d.

III. EXPERIMENTAL RESULTS

A. Qualitative description of the phase diagram

In a first step, we describe the different regimes observed in the experiment when varying the grain diameter d. We used three different grain sizes: diameters in the range 150–250, 250–425, and 425–600 μm.

For small grains (150–250 μm), when the air is injected, a large gas pocket forms below the surface. A dome growth due to the subsequent surface deformation is observed. Typically—at any given air flow Φ—the gas pocket grows for 3–5 min until the trapped air is suddenly liberated. In this case, the bubble emission at the surface occurs over a region limited by the size of the underlying gas pocket. The lower limit in the grain size can be understood as follows: when the grains are small, the Laplace overpressure γ/d is large enough to lift the whole granular column above as it exceeds the typical hydrostatic pressure $\rho_g g h_g$, where ρ_g stands for the density of the grains.

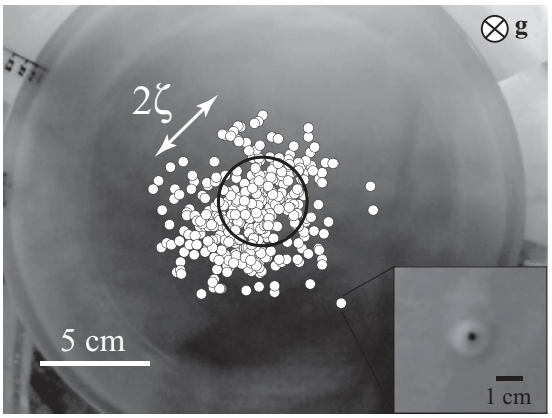

FIG. 2. Loci of the gas emissions: Each of the white circles indicates the locus of a bubble emission. Half of the bubbles were emitted in the black circle of radius ζ (Fig. 3). Inset: Example of a bubble emission (d =250–425 μm, Φ = 3 mL/s, h_g = 20 cm).

For intermediate grain size (250–425 μm), bubbles are emitted at the surface of the granular layer, without any large-scale surface deformation. Bubble emission consists of successive, single bubbles, apparently randomly distributed in space around the centered air injection point (Fig. 2).

For large grains (425–600 μm), the behavior of the system is drastically different. The air crosses the immersed grain layer easily, producing not a single but multiple simultaneous bubble emissions at its surface. This transient behavior lasts for several seconds, up to several minutes, the air flow fluidizing rapidly the granular bed in a localized region until stabilizing to a single bubble emission location at the vertical of the inlet. This regime can be understood as follows: because of the large grain size, the capillary overpressure is small, and the air flows easily between the grains. The flow rate is not negligible anymore, and one cannot consider that the system is quasistatic and neglect the charge loss in the channels formed by the gas within the grains. The air then invades the material almost in the whole available free space between the grains.

This work focuses on the venting dynamics of single, successive bubbles emitted at the free surface of an immersed granular layer. Therefore, in the following sections, we will focus on grain diameters 250–425 μm only, and analyze the bubble distribution when varying the grain height h_g.

B. Gas emission distribution

During 10 min, one observes several hundreds of events (Fig. 2). From the image analysis, we obtain the distance r separating the emission loci from the cylinder axis and report the corresponding values as a function of time t [Fig. 3(a)]. In the considered parameter range, we observe that events are widely, rather homogeneously, distributed around the vertical of the gas inlet. In addition, reporting the autocorrelation function R of the distance r [Fig. 3(b)], we observe that there does not exist any long-term correlation between the bubble emission loci. Indeed, R drops down quickly over a typical number of about two or three events, and, in any case, vanishes after 10 bubble emissions.

From the experimental data, we determine the probability distribution $p(r)$ and the associated cumulative probability $F(r) \equiv \int_0^r p(u)du$ [Fig. 3(c)]. We observe that F is rather well described by a Gaussian function [Fig. 3(c), inset]. We define the typical width ζ of the central region by $F(\zeta) \equiv 1/2$, which means that half of the bubbles escape the free surface in the circle of radius ζ at the vertical of the inlet.

It is then particularly interesting to consider the dependence of ζ on the depth h_g of the granular bed. For a given granular material, the data are compatible with $\zeta \propto \sqrt{h_g}$, as we will check in the following sections. This scaling does not depend

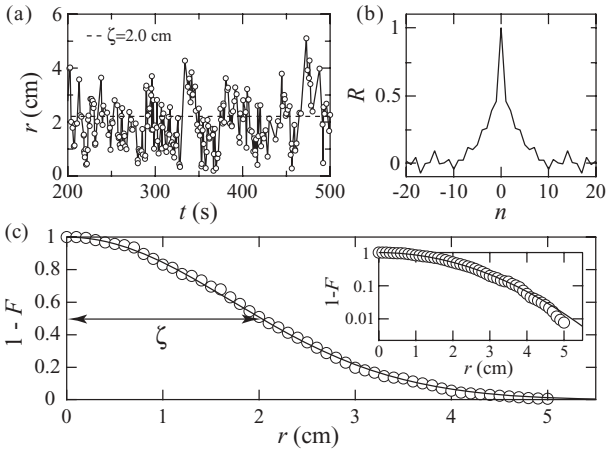

FIG. 3. (a) Distance r vs time t (data from Fig. 2). A total acquisition lasts for 10 min (300 s are displayed here). (b) Autocorrelation R of the signal as a function of the neighboring bubble number n. (c) Complementary cumulative distribution function $1 - F(r)$. The distribution is described by a Gaussian function (full line). The width at half height, 2ζ, corresponds to the diameter of the circle in which half of the bubbles are emitted. Inset: Log-lin plot of the data (circles) and Gaussian fit (full line) ($d = 250$–425 μm, $\Phi = 3$ mL/s, $h_g = 20$ cm).

significantly on the flow rate Φ (Fig. 4). In the next section, we report the results of the 2D experiment, which makes it possible to visualize the air path through the granular layer and, thus, helps to understand the empirical law $\zeta \propto \sqrt{h_g}$.

C. Additional 2D experiment

In order to directly observe the paths of air within the granular material, we designed a two-dimensional setup that consists of a vertical Hele-Shaw cell: the immersed granular matter is contained between two vertical walls (glass plates 40 cm wide, 30 cm high, gap 2 mm). In the 2D experiment, the air flow is imposed by means of a mass-flow controller (Bronkhorst, Mass-Stream Series D-5111). The flow rate Φ

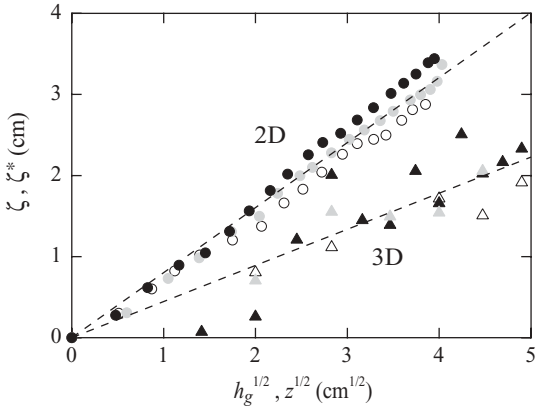

FIG. 4. Distances ζ vs $\sqrt{h_g}$ and ζ^* vs $\sqrt{z}$. In 3D (triangles), the typical size ζ of the region in which bubbles escape the free surface is compatible with the scaling $\zeta \propto \sqrt{h_g}$, independent of the flow rate Φ. In 2D (circles), accordingly, ζ^* scales like $\sqrt{z}$, almost independent of Φ [gray scale, Φ (mL/s): white, 1.0; gray, 2.0; black, 3.0 (3D experiment); white, 0.4; gray, 0.9; black, 1.3 (2D experiment); $d = 250$–425 μm.]

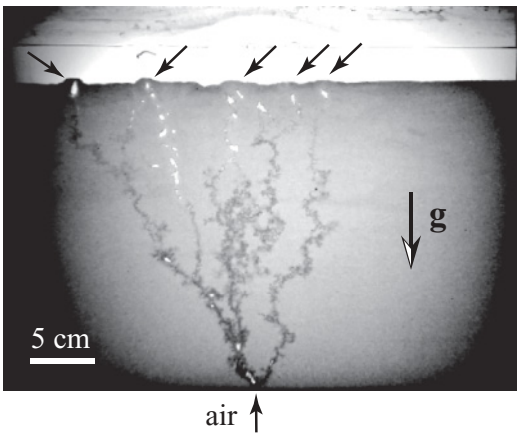

FIG. 5. Air paths observed in the 2D experiment. The air creates several paths within the granular bed and one observes several gas-emission loci at the free surface (arrows) ($h_g = 22$ cm, $h_w = 2$ cm, $d = 250$–425 μm, $\Phi = 0.43$ mL/s).

ranges from 0.2 to 2.2 mL/s. A webcam (Logitech, QuickCam Express) is used to image the system from the side, whereas the light source (transparency flat viewer, Just NormLicht, Classic Line) is positioned behind the cell. Again, the initial state of the system consists of an immersed granular bed, free of bubbles, whose surface is leveled. Air is then gently injected from an inlet at the center of the lower edge.

Direct observation from the side shows that air invades the system in two qualitatively different ways, depending on the flow rate. At small flow rate, the air does not induce any significant displacement of the grains while creating a new path and forms a rather complicated network of channels (Fig. 5). The granular material can then be, at least in the bulk, considered as a simple porous medium. However, due to local rearrangements that result from the emission of bubbles at the free surface, the channel network is permanently evolving. At a long time scale, the process leads to a region of smaller compaction at the vertical of the inlet. At larger flow rate (typically $\Phi > 1$ mL/s for $d = 250$–425 μm), one observes that the gas displaces the grains significantly while crossing the system (fingerlike behavior [16]). In this case, one usually observes the formation of a single channel that collapses after emission of the bubble at the free surface. The process repeats periodically, involving the formation of a different channel associated with each bubble.

As in the previous 3D experiment, we might determine where the bubbles are emitted at the free surface. In 2D, we chose a slightly different analysis. We suppose—and it is experimentally corroborated—that the path followed by the air in the immersed granular layer is sensitive to local conditions only (e.g., grain polydispersity and packing), and not to what lies upon it (grain height). Analyzing the air passing through a virtual horizontal line inside the 2D granular bed, located at height z, is therefore equivalent to considering the bubble emission distribution at the surface of an immersed granular layer of total height z. At long time, all the air paths create a fluidized zone (Fig. 6). Therefore, we chose to consider, in the 2D experiment, a deep immersed granular bed, and analyze the shape of the fluidized zone after injecting gas for several minutes or hours, until a steady state is reached. We can thus

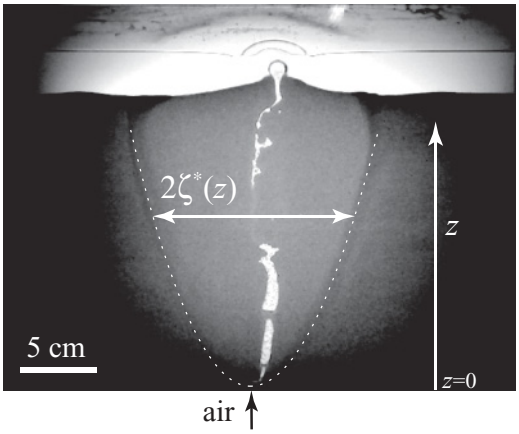

FIG. 6. Image of the fluidized region. The contrast results from the lower grain compaction in the fluidized region. Its shape is determined by image analysis, and subsequently interpolated by a parabolic function (white dashed line). We denote by $2\zeta^*(z)$ the characteristic width, in the bulk, of the region explored by the air in the stationary regime at height z ($h_g = 22$ cm, $h_w = 2$ cm, $d =$ 250–425 μm, $\Phi = 2.17$ mL/s).

access, in a single experiment, to the characteristic size $\zeta^*(z)$ of the region explored by the air as a function of the height z (Fig. 6). We observe that $\zeta^* \propto \sqrt{z}$, again independent of Φ, which is compatible with the emission of bubbles at the free surface in a region having a typical size scaling like $\sqrt{h_g}$.

In the next section, we propose a theoretical description that accounts for the parabolic shape of the region explored by the bubble paths and, thus, for the dependence of the typical size ζ on the layer thickness h_g.

IV. THEORETICAL APPROACH

In the present section, we report a simple 2D analytical model aimed at identifying the underlying mechanisms that govern the typical size ζ and show that the distribution of the bubble emission at the free surface can, as suggested by the experimental results, be accounted for by a diffusionlike process.

Qualitatively, let us consider first the propagation of air creating a path in the immersed granular material. A gas channel between the grains connects the path's upper end to the inlet at the bottom. Due to the injection at the bottom, the upper end moves when the inner overpressure overcomes the capillary overpressure associated with the narrow space between the surrounding grains. Depending on the local arrangement of the grains, the upper end can move upward or, more or less, sideward. Such a process results in a meandering of the path toward the free surface.

To describe the process more precisely, we consider, in a crude approach, that the air is creating a path in a 2D square array of grains [Figs. 7(a) and 7(b)]. To take into account the local rearrangement of the grains, we assume that the capillary overpressure associated with the possible directions of air path toward $x < 0$, δP_-; $x > 0$, δP_+; and $z > 0$, δP_z [Fig. 7(a)] are not identical but given according to a random distribution around a typical value δP_c. In such a framework, potential correlations between successive bubble emissions are

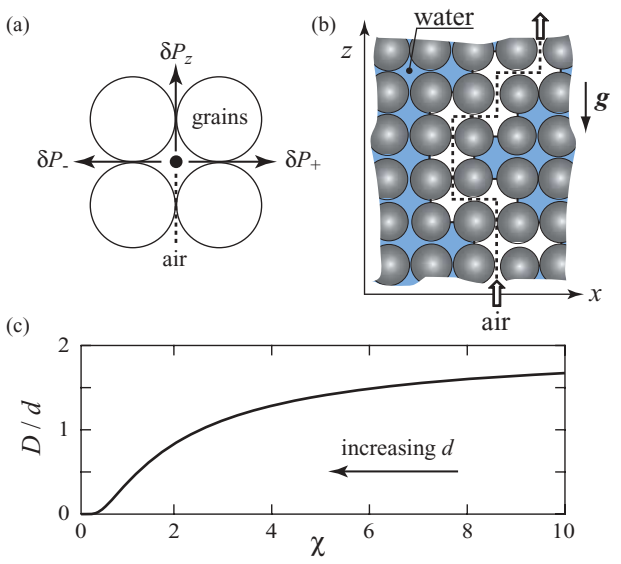

FIG. 7. (Color online) (a) Definition of the capillary pressures δP associated with the possible directions of air path after reaching a node (black dot): toward $x < 0$ (δP_-), $x > 0$ (δP_+), or $z > 0$ (δP_z). The model discards the possibility for the air to propagate downward. (b) Sketch of the considered grain arrangement. The air, injected at the bottom, propagates through the easiest path between the grains (dashed line), biased by gravity (see text). (c) Normalized coefficient D/d vs parameter χ. The coefficient D scales like the grain size and is a function of the unique parameter χ [Eqs. (1) and (4)].

neglected. Indeed, based on the experimental results reported in Fig. 3, which show that r is not correlated at long term, we can assume, in a first approximation, that each air channel forms in a medium that has not been altered by the previous one.

The system is subjected to gravity. Due to the hydrostatic equilibrium, there exists a typical pressure difference δP_g between the surrounding liquid on top and on the sides. We can estimate $\delta P_g \simeq \rho g d/2$, where g stands for the acceleration due to gravity, ρ is the density of water, and d the typical grain size.

Thus, even if the capillary overpressures δP_-, δP_+, and δP_z are equal on average, due to the hydrostatic overpressure δP_g, the upper end of the path is more likely to propagate upward. The air will propagate upward if $(\delta P_z - \delta P_g)$ is smaller than both δP_- and δP_+. Let us denote by p_z the associated probability. With such a definition, one can estimate that the upper end of the air path moves randomly N times to the left or to the right before moving once upward, with $N \sim 1/p_z - 1$. As a consequence, the lateral mean-square displacement, associated with a displacement toward the free surface of the typical size d of a grain, can be estimated to be $\langle \delta x^2 \rangle \sim N d^2$. Thus, on average, the lateral distance ζ^* between the path and the vertical of the inlet at the altitude z is given by $\zeta^* \sim \sqrt{D\,z}$, where

$$D \sim d\left(\frac{1-p_z}{p_z}\right). \tag{1}$$

Thus, a diffusionlike process accounts for the dependence of ζ^* on z and that of ζ on h_g. The associated coefficient D scales like the grain size d. However, to account for the dependence

of D on d, one must evaluate the dependence of the probability p_z on the problem parameters.

To do so, let us consider that the capillary overpressures δP_-, δP_+, and δP_z are distributed according to the distribution $Q(\delta P)$. For a given value of δP_z, the probability for δP_- and δP_+ to be larger than $(\delta P_z - \delta P_g)$ and, thus, for the air to propagate upward is $[\int_{\delta P_z-\delta P_g}^{\infty} Q(\delta P)\, d(\delta P)]^2$. Taking into account that δP_z is also distributed according to the same distribution Q, we estimate

$$p_z = \int_{-\infty}^{\infty} Q(\delta P_z) \left(\int_{\delta P_z-\delta P_g}^{\infty} Q(\delta P)\, d(\delta P) \right)^2 d(\delta P_z). \quad (2)$$

In order to better interpret the general expression (2), one can consider the case of a Gaussian distribution:

$$Q(\delta P) = \frac{1}{\sqrt{\pi}\sigma_p} \exp\left(-\frac{\delta P - \delta P_c}{\sigma_p} \right)^2. \quad (3)$$

The width σ_p then accounts for the local disorder in the granular packing. In this case, we get

$$p_z(\chi) = \frac{1}{\pi^{\frac{3}{2}}} \int_{-\infty}^{\infty} e^{-v^2} \left(\int_{v-\chi^{-1}}^{\infty} e^{-u^2} du \right)^2 dv, \quad (4)$$

where we defined $\chi \equiv \sigma_p/\delta P_g$. Thus, p_z and, as a consequence, D are functions of the unique parameter χ that compares the width of the distribution of the capillary pressure to the hydrostatic overpressure over the grain size. The dependence of the coefficient D on $d$can be easily evaluated numerically [Fig. 7(c)]: we observe that D decreases drastically when the grain size (respectively χ) is increased (respectively decreased).

V. DISCUSSION

The simplistic model presented earlier indicates that the propagation of the air within the immersed granular bed can be accounted for by a diffusionlike model. The associated coefficient $D = d\, f(\chi)$ is expected to scale like the grain size d and to depend on a unique control parameter, $\chi \equiv 2\sigma_p/(\rho g d)$, through an increasing function $f(\chi)$. In this framework, one predicts $\zeta^* \propto \sqrt{z}$, compatible with $\zeta \propto \sqrt{h_g}$, in agreement with the experimental observations.

In addition, the diffusion coefficient is predicted to drastically depend on the grain size, not only because of the prefactor but also because of the dependence of χ on d. Indeed, $\chi = 2\sigma_p/(\rho g d)$ and, furthermore, σ_p, which accounts for the distribution of the capillary overpressure, also depends on d: taking into account that the pore size (the space between the grains) is of the order of the grain size, one can estimate that the typical capillary overpressure δP_c is of the order of γ/d, where γ stands for the surface free energy of the air-water interface. Denoting by w the typical relative variation of the pore size, one can estimate further that $\sigma_p \sim w\,\gamma/d$ and, thus, that $\chi \sim 2w\gamma/(\rho g d^2)$. Thus, the control parameter χ and, in accordance, the coefficient D depend drastically on the grain size. For a granular bed made of monodisperse grains, the density can range, in practice, from that of the random loose packing, $\phi = 0.54$, to that of the random close packing, $\phi = 0.64$, so that w is of the order of a few percent. For a granular bed made of polydisperse grains, w is of the order of the relative width of the size distribution, about 25% in our typical experimental case in which d ranges from 250 to 425 μm. In this case, $\chi \sim 10$ and the model gives $D \sim 1.5\, d$. Even if we cannot expect from such a simplistic model a quantitative agreement with the experiments, we can evaluate that, for a typical depth of $h_g \sim 25$ cm, the region of the free surface in which the bubbles are expected to exit must be of the order of $\sqrt{dh_g} \sim 1$ cm, thus centimetric, in fairly good agreement with the experimental observations (Fig. 4). We remark that, for $\chi > 1$, D/d remains of the order of the unity and $\zeta \sim \sqrt{dh_g}$.

Due to the existence of very different regimes (Sec. III A), we have not been able to contrast our theoretical description with the experimental results in a large range of grain size. However, we do think that it remains valid for small grain size provided that the depth of the granular bed is large enough, so large that the capillary overpressure is not enough to lift the granular material as a whole.

The model we developed to describe the diffusionlike process is based on the hypothesis that all events (bubbles) are independent. There is, however, some correlation among the closest neighboring bubbles [Fig. 3(b)]. It points out the fact that a bubble rising in the granular medium creates a "weaker" path, that the next bubble will preferentially follow. This phenomenon has already been observed in complex fluids [17–21]. A way to improve the model could be by incorporating a weakness factor into the probabilities associated with the points in the mesh that were affected by the previous air path.

For large depth h_g (typically, $h_g > 6$ cm for $d = 250$–425 μm), we interestingly observe that, from time to time, stronger correlations between the loci of successive bubble emissions appear: the bubble emission remains in a very localized region, forming clusters of bubbles. Such events are revealed by small fluctuations of r around a finite value (Fig. 8). In this case, the air propagating through the immersed granular layer is able to create and maintain an open channel up to an intermediate height, the release of a bubble at the free surface being not enough to induce a collapse of the path along its whole length. A similar phenomenon (open channel) has already been reported, but the authors focused on the dynamics of the pressure signal in the chamber and not on the locus of the bubble emissions [11,12]. When a path partially

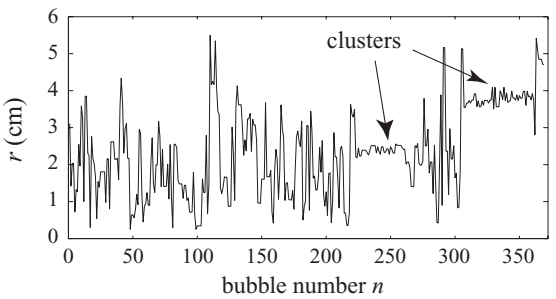

FIG. 8. Radius r vs bubble number n. For large depth, a strong correlation between successive bubbles might be observed: several successive bubbles are emitted in a narrow region (cluster) before the system turns back to the regular regime ($h_g = 14$ cm, $d = 250$–425 μm, $\Phi = 4.3$ mL/s.)

stabilizes in the bulk, the upper end of the stable path plays the role of an intermediate inlet whose depth controls the size of the narrower region in which the bubbles are emitted at the free surface. After the collapse of the whole path, the system turns back to a more regular regime until, fortuitously, a new path partially stabilizes. Thus, for large depth, one might observe at the free surface clusters of emission loci instead of one single region centered at the vertical of the inlet.

VI. CONCLUSION

We showed that the spatial distribution of the bubble emissions at the free surface of an immersed granular bed can be accounted for by a diffusionlike process. As a result, the typical size of the region in which the bubbles are emitted is directly related to the depth of the granular bed h_g and scales like $\sqrt{D\,h_g}$. The associated coefficient D scales like the typical grain size but is a rather complicated function of a unique parameter that compares the distribution of the typical capillary overpressure γ/d associated with the pores to the typical variation $\rho g d$ of the hydrostatic pressure difference over the grain size. As a result, the coefficient D is a decreasing function of the grain size: large grains lead to a narrow region at the free surface, whereas small grains tend to spread the loci of the bubble emissions. Finally, we interestingly observe that the partial stabilization of the path within the granular bed can lead to the appearance, at the free surface, of several clusters of bubble-emission loci, which might be relevant for explaining field observations [2].

The simplistic description of the model still deserves to be investigated further. To determine experimentally the relation between D and χ, taking into account that it is difficult in practice to characterize the granular bed (polydispersity and arrangement of the grains), we plan to vary, for a given granular material, the effect of gravity by tilting the 2D cell. The result of the latter study will be the subject of a future publication.

ACKNOWLEDGMENTS

G.V. acknowledges a grant by CONICYT (Comisión Nacional de Investigación Científica y Tecnológica, Gobierno de Chile). The authors are grateful to F. Vittoz, from ENS Mechanical Workshop, for the design and setup of the 2D experiment.

[1] T. Mörz, E. A. Karlik, S. Kreiter, and A. Kopf, Sediment. Geol. **196**, 251 (2007).
[2] L. Naudts, J. Greinert, Y. Artemov, S. E. Beaubien, C. Borowski, and M. De Batist, Mar. Geol. **251**, 253 (2008).
[3] G. Bohrmann, K. Heeschen, C. Jung, W. Weinrebe, B. Baranov, B. Cailleau, R. Heath, V. Hünerbach, M. Hort, D. Masson, and I. Trummer, Terra Nova **14**, 69 (2002).
[4] T. Wilhelm and K. Wilmański, Int. J. Multiphase Flow **28**, 1929 (2002).
[5] E. G. Flekkøy, A. Malthe-Sørenssen, and B. Jamtveit, J. Geophys. Res. **107**, 2151 (2002).
[6] P. Rigord, A. Guarino, V. Vidal, and J.-C. Géminard, Granular Matter **7**, 191 (2005).
[7] J. M. Valverde and A. Castellanos, Phys. Rev. E **75**, 031306 (2007).
[8] F. Zoueshtiagh and A. Merlen, Phys. Rev. E **75**, 056313 (2007).
[9] A. Mazzini, M. K. Ivanov, A. Nermoen, A. Bahr, G. Bohrmann, H. Svensen, and S. Planke, Mar. Petrol. Geol. **25**, 457 (2008).
[10] A. Vedvik, G. Wagner, U. Oxaal, J. Feder, P. Meakin, and T. Jøssang, Phys. Rev. Lett. **80**, 3065 (1998).
[11] L. Gostiaux, H. Gayvallet, and J.-C. Géminard, Granular Matter **4**, 39 (2002).
[12] G. Varas, V. Vidal, and J.-C. Géminard, Phys. Rev. E **79**, 021301 (2009).
[13] V. Vidal, G. Varas, and J.-C. Géminard, in *Compte-rendus de la 13e Rencontre du Non-Linéaire*, edited by C. Josserand, M. Lefranc, and C. Letellier (Non-Linéaire, Paris, 2010), pp. 199–204.
[14] I. Kliakhandler, Phys. Fluids **14**, 3375 (2002).
[15] T. Divoux, E. Bertin, V. Vidal, and J.-C. Géminard, Phys. Rev. E **79**, 056204 (2009).
[16] C. Chevalier, A. Lindner, M. Leroux, and E. Clément, J. Non-Newtonian Fluid Mech. **158**, 63 (2009).
[17] M. J. Riddle, C. Narvaez, and R. B. Byrd, J. Non-Newtonian Fluid Mech. **2**, 23 (1977).
[18] G. Gheissary and B. H. A. A. van den Brule, J. Non-Newtonian Fluid Mech. **67**, 1 (1996).
[19] S. Daugan, L. Talini, B. Herzhaft, and C. Allain, Eur. Phys. J. E **7**, 73 (2002).
[20] X. Frank, H. Z. Li, and D. Funfschilling, Eur. Phys. J. E **16**, 29 (2005).
[21] V. Vidal, M. Ichihara, M. Ripepe, and K. Kurita, Phys. Rev. E **80**, 066314 (2009).